Journal of Magnetic Resonance 212 (2011) 17–25

Contents lists available at ScienceDirect

Journal of Magnetic Resonance

journal homepage: www.elsevier.com/locate/jmr

Quantitative phenomenological model of the BOLD contrast mechanism

John D. Dickson [a,*], Tom W.J. Ash [b], Guy B. Williams [b], Alexander L. Sukstanskii [c], Richard E. Ansorge [a], Dmitriy A. Yablonskiy [c]

[a] Department of Physics, Cavendish Laboratory, Cambridge University, Cambridge, UK
[b] Wolfson Brain Imaging Centre, University of Cambridge School of Clinical Medicine, Cambridge, UK
[c] Mallinckrodt Institute of Radiology, Washington University, St. Louis, MO, USA

ARTICLE INFO

Article history:
Received 9 April 2011
Revised 2 June 2011
Available online 13 June 2011

Keywords:
BOLD fMRI
BOLD modelling
Quantitative BOLD

ABSTRACT

Different theoretical models of the BOLD contrast mechanism are used for many applications including BOLD quantification (qBOLD) and vessel size imaging, both in health and disease. Each model simplifies the system under consideration, making approximations about the structure of the blood vessel network and diffusion of water molecules through inhomogeneities in the magnetic field created by deoxyhemoglobin-containing blood vessels. In this study, Monte-Carlo methods are used to simulate the BOLD MR signal generated by diffusing water molecules in the presence of long, cylindrical blood vessels. Using these simulations we introduce a new, phenomenological model that is far more accurate over a range of blood oxygenation levels and blood vessel radii than existing models. This model could be used to extract physiological parameters of the blood vessel network from experimental data in BOLD-based experiments. We use our model to establish ranges of validity for the existing analytical models of Yablonskiy and Haacke, Kiselev and Posse, Sukstanskii and Yablonskiy (extended to the case of arbitrary time in the spin echo sequence) and Bauer et al. (extended to the case of randomly oriented cylinders). Although these models are shown to be accurate in the limits of diffusion under which they were derived, none of them is accurate for the whole physiological range of blood vessels radii and blood oxygenation levels. We also show the extent of systematic errors that are introduced due to the approximations of these models when used for BOLD signal quantification.

1. Introduction

Analytical modelling of NMR signal formation in the presence of a blood vessel network has been attempted many times since the discovery of BOLD contrast [1,2]. For the static dephasing regime (zero diffusion) a model was introduced by Yablonskiy and Haacke that explained some of the major features of the phenomenon [3]. In particular, the dependence on the susceptibility of the blood vessel network and its fractional occupancy, the discovery of which allows the oxygenation and volume fraction of deoxygenated blood to be measured separately in the brain [4,5]. This is an important finding as quantitative measures of blood oxygenation represent a rational means of evaluating tissue ischemia [6,7] and hypoxia [8,9].

A number of models that attempt to improve on the results of the Yablonskiy and Haacke model by introducing diffusion to the model have since been proposed. One advantage to this approach is that it elucidated the dependence on blood vessel radius which has led to the emergence of vessel size imaging [10,11]. The ability to measure vessel radii in vivo has obvious implications in the study of angiogenesis and vascular normalisation in tumour studies [12,13]. However, all "diffusive models" of the BOLD mechanism have made assumptions in their derivation that limit the range of vessel radii for which they are valid. In most cases, the exact criteria for validity are unclear.

Using Monte Carlo methods it is possible to directly simulate the BOLD signal for any tissue and pulse sequence parameters with equal accuracy. Studies taking this approach [14–16] have increased understanding of the link between BOLD signal and the underlying hemodynamics, which in turn has influenced fMRI experimentation design. However, such numerical models have not allowed the contributions of the various signal decay mechanisms to be separated. Application of these models therefore typically involves interpolation [15] or extrapolation [17] of high dimensional lookup tables which means that they are not as transferable as analytical models.

In this study we use Monte-Carlo simulation methods to show the validity criteria of a number of models from the literature. We then use simulation results to construct a simple phenomenological model that is extremely accurate for the physiological range of blood oxygenation, blood volume and vessel radii.

* Corresponding author. Address: Cavendish Laboratory, JJ Thomson Avenue, Cambridge CB3 0HE, UK.
E-mail address: jdd36@cam.ac.uk (J.D. Dickson).

1090-7807/$ - see front matter © 2011 Elsevier Inc. All rights reserved.
doi:10.1016/j.jmr.2011.06.003

2. Theory

The basic physics behind the BOLD mechanism is well understood. Blood vessels containing paramagnetic deoxyhaemoglobin induce extravascular local field inhomogeneities, which cause spins of protons in the system to sustain differing phase shifts ϕ, and hence create MR signal decay. The signal remaining at time t after excitation is given by the average of the contributions from protons across the volume

$$s(t) = \langle \exp(i\phi(t)) \rangle, \tag{1}$$

where because magnetic fields obey linear superposition, a proton's phase can be found by integrating the sum of frequency shifts $\omega_n(t)$ caused by all N vessels over time

$$\phi(t) = \int_0^t dt' \sum_{n=1}^{N} \omega_n(t'). \tag{2}$$

In this equation time dependence of frequency shifts $\omega_n(t)$ is due to the water molecule's diffusion in the inhomogeneous field. If blood vessels are assumed to be infinite cylinders of uniform susceptibility, then the frequency contribution to an extravascular proton at distance r from the centre of a cylinder is given by:

$$\omega(r,\theta,\varphi) = \begin{cases} \delta\omega\left(\cos^2\theta - \frac{1}{3}\right) & r < R \\ \delta\omega \frac{R^2}{r^2} \cos 2\varphi \sin^2\theta & r > R \end{cases}, \tag{3}$$

where R is the vessel radius, θ is the angle between the vessel and the B_0 field and φ is the azimuthal angle of the proton position in a plane perpendicular to the vessel (not to be confused with the phase ϕ). $\delta\omega$ is the characteristic frequency shift (i.e. $\omega(R, \pi/2, 0)$) and can be found from

$$\delta\omega = 2\pi\gamma B_0 \Delta\chi_0 Hct(1 - Y), \tag{4}$$

where $\Delta\chi_0$ is the difference in susceptibility between entirely oxygenated and entirely deoxygenated red blood cells, Hct is the blood hematocrit, Y is the blood oxygenation level ($Y = 1$ for fully oxygenated blood and $Y = 0$ for fully deoxygenated blood). In case when arterial blood is fully oxygenated the value $(1 - Y)$ coincides with the oxygen extraction fraction OEF. In this study we assume cerebral $Hct = 0.34$ [17], $\Delta\chi_0 = 0.264 \times 10^{-6}$ [18].

2.1. The Yablonskiy and Haacke model (static dephasing regime) (3)

This model was derived in the static dephasing regime which means that diffusion is considered to be zero. If the vessel network is assumed to be composed of randomly oriented vessels, the BOLD signal can be found from Eqs. (2)–(4) by taking the limit as the number of vessels N and system volume V_0 approach infinity (their ratio V_0/N remains constant) and averaging over all possible proton positions, vessel positions and vessel orientation angles

$$s_0(t) = \lim_{N\to\infty} \int_{V_0} \frac{d^3\mathbf{r}}{V_0} \left\langle \exp\left[-\sum_{n=1}^{N} i\omega_n(\mathbf{r})t \right] \right\rangle, \tag{5}$$

where s_0 denotes the signal in the static dephasing regime. In the case of blood vessels with a uniform orientation distribution, this expression can be reduced to the following, rather simple equation [3]:

$$s_0(t) = \exp\left(-\frac{\zeta}{3} \int_0^1 du(2+u)\sqrt{1-u} \frac{1 - J_0(\delta\omega t u)}{u^2} \right), \tag{6}$$

where J_0 is the zero order Bessel function, ζ is the volume fraction occupied by deoxyhaemoglobin-containing cylinders (the deoxygenated Cerebral Blood Volume, dCBV). Equation (6) can also be presented as

$$s_0(t) = \exp\left[-\zeta \left({}_1F_2\left(\left\{ -\frac{1}{2} \right\}; \left\{ \frac{3}{4}, \frac{5}{4} \right\}; -\frac{\delta\omega^2 t^2}{4} \right) - 1 \right) \right], \tag{7}$$

where ${}_pF_q$ is the extended hypergeometric function. For the spin-echo sequence with spin echo time TE, t should be replaced by $|t - TE|$. Note that in this approximation the signal decay depends only on total dCBV and not the vessel radii. Also note that equations in this paper may appear to differ from those in the cited articles due to the varying definitions of $\delta\omega$.

2.2. The Kiselev and Posse model (linear local field approximation) (19)

To include diffusion in their model, Kiselev and Posse make use of the solution to the Bloch–Torrey equation for the case of linear local field variations. The result is that the signal in Eq. (1) can be approximated to

$$s(t) = \left\langle \exp\left(-i\omega(\mathbf{r})t - \frac{D}{3}[\nabla\omega(\mathbf{r})]^2 t^3 \right) \right\rangle. \tag{8}$$

Following this through as before, the final expression for the signal is

$$s(t) = \exp\left(-\zeta \int_0^{\pi} \frac{\sin\theta d\theta}{2} \int_0^1 \frac{du}{u^2} \left[1 - \exp\left(-\frac{4D}{3R^2} \delta\omega^2 t^3 u^3 \sin^4\theta \right) J_0(\delta\omega t u \sin^2\theta) \right] \right), \tag{9}$$

where D is the diffusion coefficient of water in tissue. The expression for the signal in the presence of a spin echo is given in Ref. [19] (in which Eq. (9) is misprinted with a positive exponent).

Kiselev and Posse have also introduced a model for the case of fast diffusion (the Diffusion Narrowing Regime or DNR) [20] by solving the Bloch–Torrey equations with second order perturbation theory. This model is valid for the case of fast diffusion in the same way as the Sukstanskii and Yablonskiy model [21,22], hence has very similar asymptotic forms and will not be explored here.

2.3. The Sukstanskii and Yablonskiy model (Gaussian phase approximation) [21,22]

To create a model of BOLD signal for the case of fast diffusion, Sukstanskii and Yablonskiy made the assumption that the phases of spins in the system follow a Gaussian distribution [21,22]. This allows Eq. (1) to be approximated to

$$\begin{aligned} s(t) &= \exp\left(-\tfrac{1}{2}\langle \phi^2(t) \rangle \right), \\ &= \exp\left(-\int_0^t dt'(t - t')G(t') \right), \end{aligned} \tag{10}$$

where $G(t)$ is the frequency correlation function given by

$$G(t) = \langle \omega(0)\omega(t) \rangle = \langle \omega(\mathbf{r})\omega(\mathbf{r})P(\mathbf{r}, \mathbf{r}_0, t) \rangle. \tag{11}$$

In the above, $P(\mathbf{r}, \mathbf{r}_0, t)$ is the probability of diffusing from $\mathbf{r}$ to $\mathbf{r}_0$ in time t (this would be a simple Gaussian if diffusion were not restricted) and the angular brackets refer to an average over proton positions, vessel positions and vessel orientations. For the case of impermeable cylinders we arrive at the following expression for the signal

$$s(t) = \exp\left(-\frac{128\zeta\delta\omega^2 t_D^2}{15\pi^2} \int_0^{\infty} d\nu \frac{g(\nu^2 t/t_D)}{\nu^9 [J_2'^2(\nu) + N_2'^2(\nu)]} \right), \tag{12}$$

where $J'(\nu)$, and $N'(\nu)$ are first derivatives of Bessel functions of the first and second kinds respectively and, for the case of the FID sequence, the function g is given by

$$g_{FID}(x) = \exp(-x) + x - 1. \tag{13}$$

To allow full comparison with the previous models, this is extended to arbitrary time in the spin echo sequence in the results section.

Sukstanskii and Yablonskiy also derived an expression for the intravascular signal, where ω is given by Eq. (3) ($r < R$). In the intravascular space, ω is independent of R, r and φ, therefore the only averaging necessary is over vessel orientation angle:

$$s_{iv}(t) = \int_0^{\pi} \frac{\sin\theta d\theta}{2} \exp\left[-i\delta\omega t\left(\cos^2\theta - \frac{1}{3}\right)\right] = \left(\frac{\pi}{2\delta\omega|t|}\right)^{1/2} \exp\left(\frac{i\delta\omega t}{3}\right)\left[C\left(\left|\frac{2\delta\omega t}{\pi}\right|^{1/2}\right) - i\,\mathrm{sign}(t)S\left(\left|\frac{2\delta\omega t}{\pi}\right|^{1/2}\right)\right], \quad (14)$$

where $S(x)$ and $C(x)$ are the Fresnel functions (defined here according to Abramovitz and Stegun [23]), respectively, sign(x) is a sign function and the factor $\sin\theta/2$ accounts for the probability distribution of vessel orientation angles. We include this model for completeness, however it is not explored as this work concerns only the extravascular signal.

2.4. The Bauer et al. Model (strong-collision approximation) (24, 25)

Bauer and colleagues originally introduced this model for the myocardium where blood vessels may be considered to be parallel. In the results section we extend it to the case of random cylinders to make it relevant to the case of BOLD signal in the brain. Here we first show it as it was originally derived [24].

In order to find the signal in the presence of diffusion, the authors first find the Laplace transform of the signal in the static regime (the signal from the Yablonskiy and Haacke model)

$$\hat{s}_0(s) = \int_V d^3\mathbf{r}\frac{1}{s - i\omega(\mathbf{r})}, = \frac{1}{(1-\zeta)s}\left[H_C\left(\frac{s}{\zeta\delta\omega}\right) - \zeta H_C\left(\frac{s}{\delta\omega}\right)\right], \quad (15)$$

where the function H is specific to the geometry of the field perturber. For the case of parallel cylinders, the H function is given by

$$H_c(y) = \left(1 + \frac{\sin^4\theta}{y^2}\right)^{1/2}. \quad (16)$$

Under the strong-collision approximation, the frequency distribution in the presence of diffusion can then be found using the expression

$$p(\omega) = \frac{1}{\pi}\left|\mathrm{Re}\frac{\hat{s}_0(i\omega + \tau_c^{-1})}{1 - \tau_c^{-1}\hat{s}_0(i\omega + \tau_c^{-1})}\right|, \quad (17)$$

where for the case of impermeable cylinders, τ_c is given by

$$\tau_c = \frac{R^2}{4D}\cdot\frac{\ln|\zeta|}{(1-\zeta)}. \quad (18)$$

Finally, the signal in the diffusive regime is found by Fourier transform of the distribution of frequency states.

$$s(t) = \int_{-\infty}^{\infty} d\omega p(\omega)\exp(i\omega t). \quad (19)$$

Eqs. (15)–(19) are derived in [24,25] for the FID signal. For the signal at the spin echo time ($t = TE$), the expression was derived in Ref. [25].

2.5. Monte Carlo simulations

In order for simulation and theoretical results to be directly comparable, simulations were performed under the same approximations as previously described [26]. The vessel network was simulated by randomly selecting starting points in a sphere and extending them out to the surface in random orientations. Half of the starting points were on the surface of the sphere and half within the volume as this method produced the highest homogeneity of vessel density [26].

For simulations with realistic vessel radii we assumed the distribution given in Ref. [27]:

$$P\left(\frac{1}{\sqrt{2R}}\right) = \begin{cases} N(0.38, 4.9\times10^{-3}) & 0 < R < 25\ \mu\mathrm{m} \\ 0 & \text{otherwise} \end{cases} \quad (20)$$

where $N(\mu, \sigma^2)$ is a normal distribution with mean μ and variance σ^2. This distribution can be split into capillaries and veins by making the assumption that capillaries are symmetrically distributed about a mean of 3.235 μm [27]. From these distributions, the blood volume corresponding to a given radius of the containing vessels is: $\zeta(R) = R^2P(R)/C$ where C is the normalisation constant: $C = \int_0^{R_{\max}} R^2 P(R)dR/\zeta_{\mathrm{total}}$ (see Fig. 1).

Vessels were added and assigned radii by sampling from the relevant distribution until the target ζ was reached. Then protons were added to the system in random locations near the centre of the sphere as this region had the highest homogeneity of vessel density. A 3D rendering of section of simulation space with a physiological distribution of vessel radii is given in Fig. 2. Note that the region shown represents only a tiny fraction of the total simulated volume.

At each time-point the protons were moved in each dimension by a step that was randomly sampled from the distribution $N(0, 2D\delta t)$ where δt is the time interval. If the step brought a proton into contact with a vessel it was mirror-reflected from the surface, since the vessels are assumed to be impermeable. The effect of vessel permeability was tested and found to have only a minor impact on signal formation, in agreement with Ref. [14]

The signal was calculated from the discretised versions of Eqs. (1) and (2)

$$s(t) = \frac{1}{P}\sum_{p=1}^{P}\exp(i\phi_p), \quad \phi_p = \sum_{m=1}^{t/\delta t}\sum_{n=1}^{N}\omega_{mpn}\delta t_{pn}, \quad (21)$$

where ω_{vpm} is the precession frequency contribution of vessel n (of a total N) on proton p (of a total P) at time-point m (of a total $t/\delta t$ at time t) (defined in Eqs. (3) and (4)). To simulate a spin echo, the sign of ω was reversed for $t > TE/2$.

The number of protons per simulation was 10,000. At the beginning of every simulation, protons were placed in random locations within 3 mm of the centre of the network which itself had a radius of 50–400 mm, increasing with the vessel radius. The default value of the time-step δt was 250 μs but this was subdivided into intervals of 25 μs for any proton-vessel pair with $R^2/r^2 > 0.04$. Vessels that did not pass within 3 mm of a proton were assumed to have

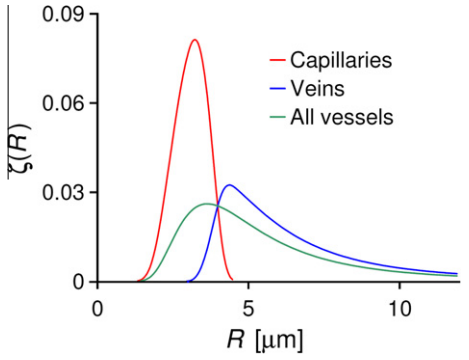

Fig. 1. Probability of blood volume as a function of the radius of its containing vessel.

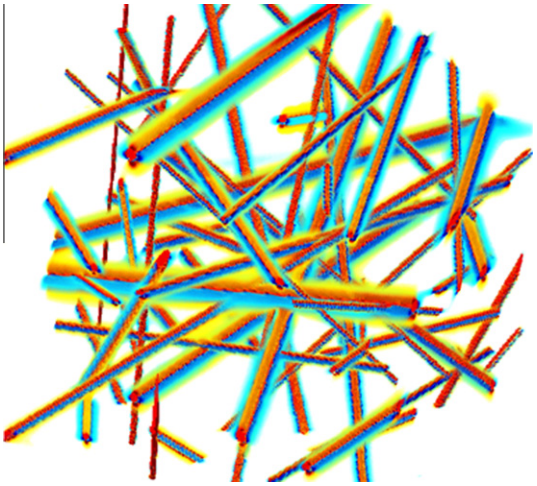

Fig. 2. Field in the simulated vessel network. Green–Blue corresponds to negative contributions and yellow–red corresponds to positive contributions. (For interpretation of the references to colour in this figure legend, the reader is referred to the web version of this article.)

no net effect on precession frequency, and only the effects of those within 1 mm were recalculated at every time-step. The list of vessels for which this was the case was refreshed for all protons after any proton had moved a distance greater than 0.03 mm. These time-saving measures were tested and found to have negligible effect on the resultant signal. Simulations were repeated 8–24 times, increasing with vessel radius to prevent increase in errors due to reduced averaging of vessel contributions with fewer vessels.

All simulation code was written in C++ and parallelised with MPI (Message Passing Interface). Some routines were based on code from Numerical Recipes in C++ (Cambridge University Press, 2002).

3. Results

First, we compare the results of the computer simulations with predictions of different theoretical models described above. The physiological parameter values used throughout this section are typical for the normal brain: $OEF = 0.4$, dCBV = 0.03; The spin echo time is $TE = 60$ ms as is typical in experimental settings [4,26].

No changes were made to the original Kiselev and Posse model as it could be directly compared to our simulation results in its original form (only the misprint in the sign in Eq. (9) was corrected). Results are presented in Fig 3.

In order to calculate the signal after the refocusing 180° RF pulse ($t > TE/2$) using the Sukstanskii and Yablonskiy model we have generalised the function g in Eq. (12) to:

$$g(t,x) = 2\exp\left(-\frac{x^2 TE}{2\tau_D}\right) + 2\exp\left(-\frac{x^2(2t+TE)}{2\tau_D}\right) - \exp\left(-\frac{x^2(t+TE)}{\tau_D}\right) + \frac{x^2(t+TE)}{\tau_D} - 3. \quad (22)$$

The resulting model is compared to simulated time-courses for a range of vessel radii in Fig 4.

Before the model of Bauer et al. could be compared to the BOLD simulations it had to be extended to the case of randomly oriented cylinders. To achieve this, the H-function in Eq. (16) was averaged over vessel orientation angle as follows

$$\widehat{s}_0(s) = \int_0^\pi d\theta \frac{\sin\theta}{2} \int_V \mathrm{d}^3\mathbf{r} \frac{1}{s - i\omega(\mathbf{r})}, = \frac{1}{(1-\zeta)s}\left[H_{RC}\left(\frac{s}{\zeta\delta\omega}\right) - \zeta H_{RC}\left(\frac{s}{\delta\omega}\right)\right], \quad (23)$$

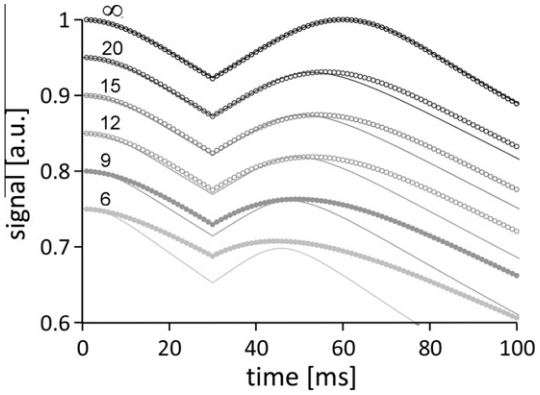

Fig. 3. Comparison of the Kiselev and Posse model with simulation results. Markers are simulated data, solid lines are theoretical curves. To better display results, signals corresponding to different R (displayed in micrometer values on the chart) are normalised to different initial amplitudes $S(0)$. The input parameters for all simulations were $OEF = 0.4$, dCBV = 0.03. The model captures the shift of the signal peak around spin echo relatively well, but not the signal behaviour around the spin echo, even for rather large vessel radii. There is only perfect agreement when $R \to \infty$. In this case diffusion does not play any role (static dephasing regime), at which point the model is identical to that of Yablonskiy and Haacke.

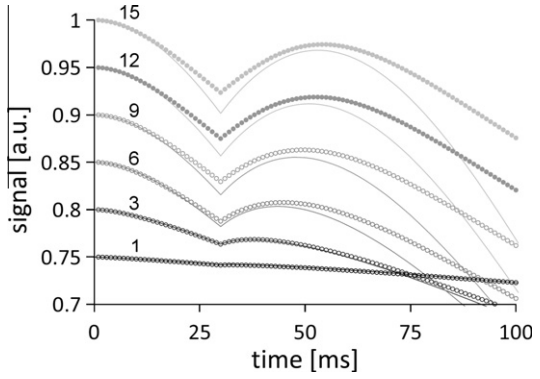

Fig. 4. Comparison of the Sukstanskii and Yablonskiy model and simulation results. Markers are simulated data, solid lines are theoretical curves. To better display results, signals corresponding to different R (displayed in micrometer values on the chart) are normalised to different initial amplitudes $S(0)$. The input parameters for all simulations were $OEF = 0.4$, dCBV = 0.03. Good agreement is seen for low vessel radius and short time, as expected under the Gaussian approximation.

$$H_{RC}(y) = \int_0^\pi d\theta \frac{\sin\theta}{2} \cdot \left(1 + \frac{\sin^4\theta}{y^2}\right)^{1/2} = {}_3F_2\left(\left\{-\frac{1}{2}, \frac{1}{2}, 1\right\}, \left\{\frac{3}{4}, \frac{5}{4}\right\}; -\frac{1}{y^2}\right). \quad (24)$$

This model is compared to our simulation results in Fig. 5. However, although it is possible to calculate the signal at the moment of the spin-echo with this model, it is not currently possible to calculate it at arbitrary times for $t > TE/2$ and so only the FID range is shown.

To compare these models in the context of vessel size imaging, we plot the impact of the vessel network on the relaxation time $\Delta R_2 = -\log(s(t))/t$ as function of the vessel radius for $t = 30$ ms (FID) and $\Delta R_2 = -\log(s(TE))/TE$ for $TE = 60$ ms (SE).

From Fig. 6 we see that the most accurate model for $R < 5$ μm is that of Sukstanskii and Yablonskiy for both the FID and SE cases. For $R > 7$ μm the extended Bauer et al. model is the most accurate for the FID case and for $R > 20$ μm the Kiselev and Posse model is most accurate for the SE case but no model is at all accurate in

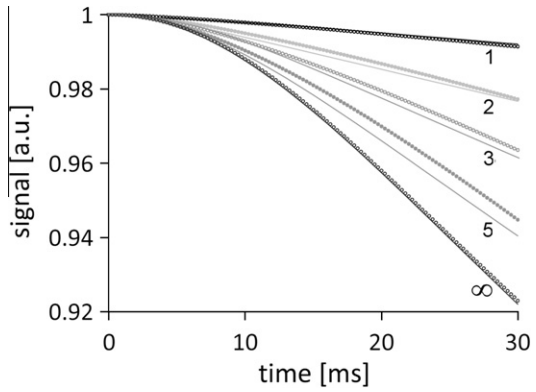

Fig. 5. Comparison of the Bauer model with simulation results. Markers are simulated data, solid lines are theoretical curves. R values are displayed in micrometer values on the chart. The input parameters for all simulations were $OEF = 0.4$, dCBV = 0.03. Relatively good agreement is seen for very large and very small (1 μm) vessels but not in the intermediate range.

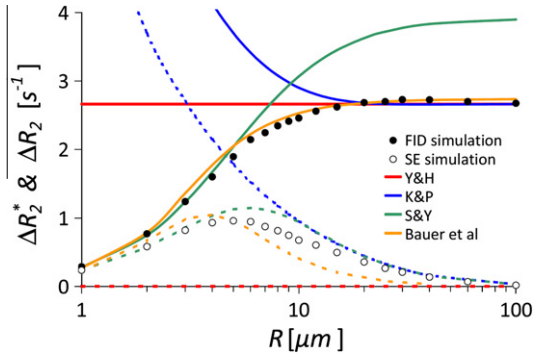

Fig. 6. The effect of vessel radius on transverse relaxation for all BOLD models. Solid and dashed lines represent model results in the FID and SE sequences respectively. Red lines – Yablonskiy and Haacke model; blue lines – Kiselev and Posse model; green lines – Sukstanskii and Yablonskiy model; orange lines – extended model by Bauer et al. Input parameters for all simulations are: $OEF = 0.4$, dCBV = 0.03. (For interpretation of the references to colour in this figure legend, the reader is referred to the web version of this article.)

the intermediate range. As the majority of the $\zeta(R)$ distribution falls into this category it may be assumed that no model tested would be accurate for a physiological distribution of radii.

It is also possible to compare the BOLD models on their ability to estimate the parameters *OEF* and dCBV in quantitative BOLD by fitting them to our simulation results. Since in any real experiment one is unable to exclude the effect of T_2 decay, we have also allowed for a shift in the measured decay rate, ΔR_2. The full model fitted was therefore $S(t) = S_0 \exp(-\delta R_2 t) s(t)$, where $s(t)$ is the BOLD signal predicted by each of the models in Eqs. (6), (9), (12), and (19).

In the Sukstanskii and Yablonskiy model, *OEF* and dCBV only appear in the coefficient G_0 and it was therefore not possible to fit these parameters separately. Instead we fitted the *OEF* on the assumption that the dCBV is known. It was also not possible to fit the Bauer model to our simulation results due to the computation time required to calculate an integral over a hypergeometric function. The process can be accelerated by creating a lookup table of timecourses over a range of *OEF*, dCBV and R values, which could then be interpolated in data fitting. However, even this process was prohibitively time-consuming for the purposes of this study. The ability of the remaining models to correctly determine the blood oxygenation and volume of our simulated curves are compared in Fig 7.

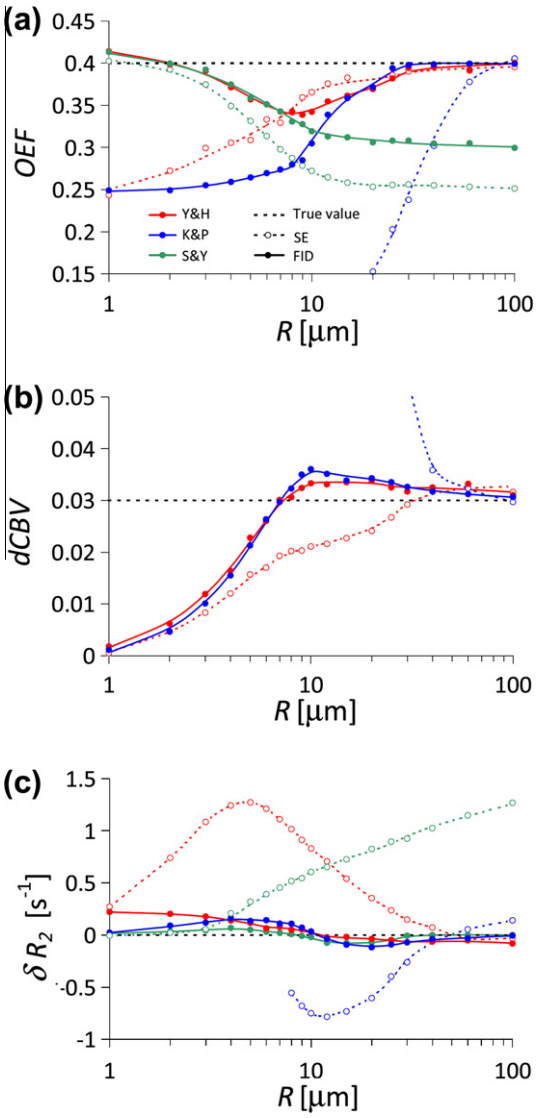

Fig. 7. Values of (a) *OEF*, (b) dCBV and (c) δR_2 found when fitting the model $S(t) = S_0 \exp(-\delta R_2 t)\, s(t)$ to simulated datasets over a range of blood vessel radius and using a variety of BOLD models, $s(t)$. The input parameters for all simulations are: $OEF = 0.4$, dCBV = 0.03, $\delta R_2 = 0$ (shown by dotted gray lines). Unlike in other figures, the lines are only shown to display trends. Solid lines represent model results in the FID sequence and dashed lines represent model results in the SE sequence. Red lines – Yablonskiy and Haacke model; blue lines – Kiselev and Posse model; green lines – Sukstanskii and Yablonskiy model (in which we assume that dCBV is known from independent measurement). Using the Kiselev and Posse SE model the optimisation failed to converge for $R \leqslant 8$ μm. (For interpretation of the references to colour in this figure legend, the reader is referred to the web version of this article.)

3.1. Phenomenological model

Analyzing simulated data we found that they can be well described by the following phenomenological equation:

$$s(t) = \exp[-\zeta f(t)], \quad f(t) = A_1(\exp[-A_2 t] - 1) + A_3 t + A_4, \tag{25}$$

where parameters A_n were all found to follow the equation

$$A_n = OEF(B_1 - B_2 \exp(-B_3 OEF)), \tag{26}$$

Except that in the FID range it was not necessary to fit A_4 as $s(0) = 1$. Results of fitting Eq. (25) to data simulated with a physiological distribution of vessel radii are shown in Fig. 8a and results of fitting Eq. (26) fitted to the resulting parameters, A_n are shown in Fig. 9a. Val-

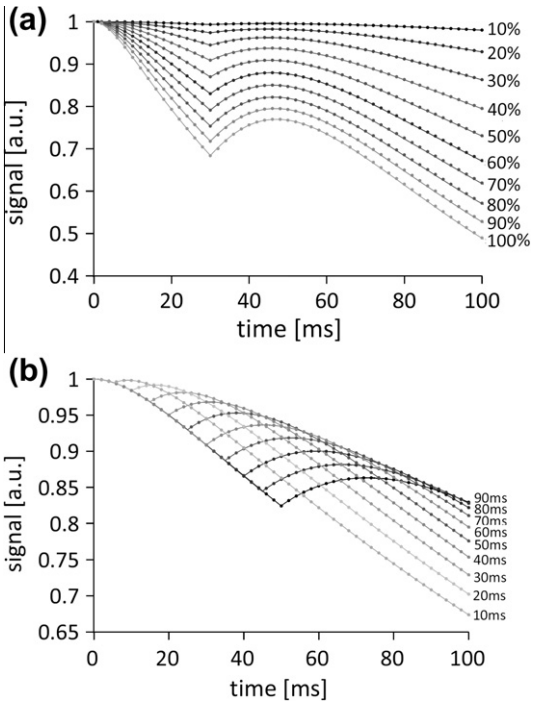

Fig. 8. (a) Phenomenological model fit to simulation results for (a) varied *OEF*, *TE* = 60 ms and (b) varied *TE* (values shown next to the curves), *OEF* = 0.40. dCBV = 0.05.

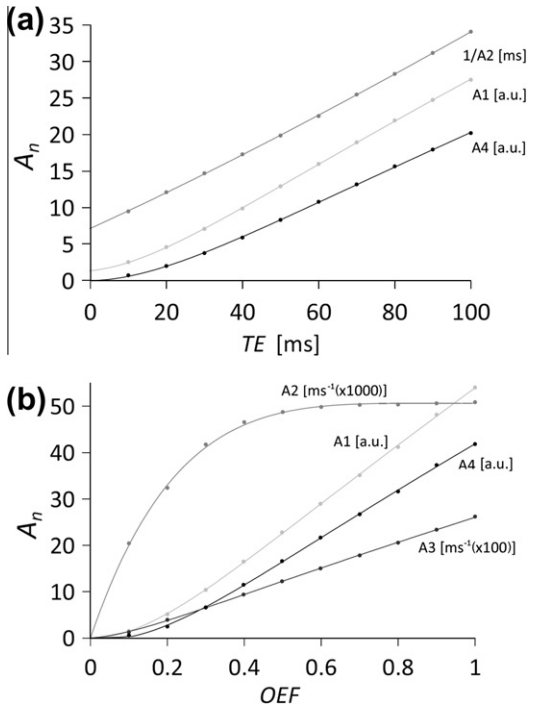

Fig. 9. Parameters in Eq. (25) found from fitting to simulation results for varied *OEF* (a) and spin-echo time (where A_3 always equals 0.48) (b). Lines are the fit to Eqs. (26) and (27) in (a) and (b) respectively.

ues of the fitted parameters are shown in Tables 1 and 2 for the FID and SE sequences respectively.

It is also possible to fit Eq. (25) to simulated data with varied spin echo time, replacing Eq. (26) with:

$$A_n = TE(B_1 - B_2\exp(-B_3 TE)) + B_4. \tag{27}$$

Table 1
Values of parameters when fitting Eqs. (25) and (26) to simulated FID timecourses using a physiological distribution of radii, *OEF* = 0–100%.

	A_1	A_2	A_3
B_1	55.385	35.314	0.3172
B_2	52.719	34.989	0.3060
B_3	−0.0242	−0.0034	3.1187

Table 2
Values of parameters when fitting Eqs. (25) and (26) to simulated GESSE timecourses using a physiological distribution of radii, *OEF* = 0–100%, $t > TE/2$ and *TE* = 60 ms.

	A_1	A_2	A_3	A_4
B_1	70.428	0.0324	0.2587	58.110
B_2	57.789	−0.1708	0.1752	62.892
B_3	1.4565	2.1357	6.1483	1.5827

However, when varying *TE* it is not necessary to fit A_3, as this parameter merely represents the long-time asymptotic decay rate. The results of this process are shown in Figs. 8b and 9b.

The phenomenological model was equally accurate under variation of the deoxygenated blood volume (results not shown). In fact the factorization of ζ was found to be accurate even when splitting the radius distribution into components. The signal was simulated for the complete distribution and then the distributions for veins and capillaries separately. The product of the signals from the two separate fractions was found to exactly match the signal from the combined distribution, which suggests that the following equation is exact for all diffusion rates [19]:

$$s(t) = \exp\left(-\int_0^\infty f(t;R)\zeta(R)dR\right) \tag{28}$$

where $f(t;R)$ is a radius-specific form function.

4. Discussion

The first result of this study was to show the ranges of validity of various resting-state BOLD models from the literature. The first diffusive model tested was the Kiselev and Posse model, which makes the assumption that local field inhomogeneities can be considered to be linear. In their paper they give the validity criterion $R \gg \sqrt{Dt}$ which translates to $R \gg 7.7$ μm for $D = 1$ μm^2 ms^{-1} and *TE* = 60 ms. Comparing their predicted decay rates with those from the simulation study in Ref. [19] suggests that this could be relaxed to simply $R > \sqrt{Dt}$, however from the curves in Fig. 3 it would seem that $R > 3\sqrt{Dt}$ would be more accurate. This disagreement is presumably due to the fact that this study has only considered the extravascular signal while Kiselev and Posse also considered intravascular signal, for which diffusion is unimportant due to the uniform cylinder approximation.

The model of Sukstanskii and Yablonskiy was derived on the assumption that the distribution of phases in the system can be represented by a Gaussian function. This is known to be valid for fast diffusion and short times and the results in Fig. 4 agree with this observation. The authors derive the following criterion for validity:

$$R < \left(\frac{\zeta D}{\delta\omega}\right)^{1/2}, \tag{29}$$

which, for the parameters in this study equates to $R < 5$ μm (as it did in theirs). The results of our simulations support this limit on

the vessel radius but also suggest that this could be extended for short times. For example, in CGS units:

$$tR < 0.03\left(\frac{\zeta D}{\delta\omega}\right)^{1/2}. \quad (30)$$

The model by Bauer et al. makes the strong collision approximation which is valid when diffusion can be considered to be a stationary Markov process, i.e. when the time scale of diffusion is much less than that of dephasing. In addition, as the diffusion coefficient approaches zero, the Bauer model converges with the static model which is known to be precise ($\tau_c \to \infty$ in Eq. [17]). In Ref. [25] the authors state that their model can therefore be seen as interpolating between the two limiting diffusion regimes. Since the analytical expression for this model exists only for the FID signal. We were not able to test it for the MR signal around the spin echo. For the FID signal, Fig. 5 shows that, although the model does work well in the limiting cases, it does not accurately map the intermediate range. There are no existing validity criteria for the Bauer et al. model that are appropriate to our simulation parameters but observation of Fig. 5 suggests that for the FID signal and typical *OEF* and dCBV values, the Bauer et al. model is accurate with vessel radii $R < 3$ μm and $R > 7$ μm.

From inspection of Fig. 6 we can see that for typical values of *OEF*, ζ and *TE*, no model is accurate in the range 4 μm $\leqslant R \leqslant$ 8 μm in the FID case and 4 μm $\leqslant R \leqslant$ 20 μm in the SE case. By comparing time-courses simulated for distributions of radii and single values we find that capillaries and veins behave approximately as though they had a single radius of $R = 3$ μm and $R = 7$ μm respectively (see Fig. 10). This means that the Sukstanskii and Yablonskiy model is able to provide an accurate representation for the case of capillaries but no model can achieve this for veins (or therefore the full distribution).

The models explored in this study are currently used for a range of applications. One such application is known as quantitative BOLD (qBOLD), in which a BOLD model is fitted to the spin echo time-course measured by the Gradient Echo Sampling of a Spin Echo (GESSE) sequence [28], thus providing measurements of the local *OEF* and dCBV, [4,5]. These parameters are of clinical significance as they provide insight into tissue ischemia and could potentially be utilised for calibrated fMRI [29–31]. By fitting the various models in the literature to our simulation results we were able to show the impact of each model's diffusion approximations on its ability to quantify blood oxygenation and volume.

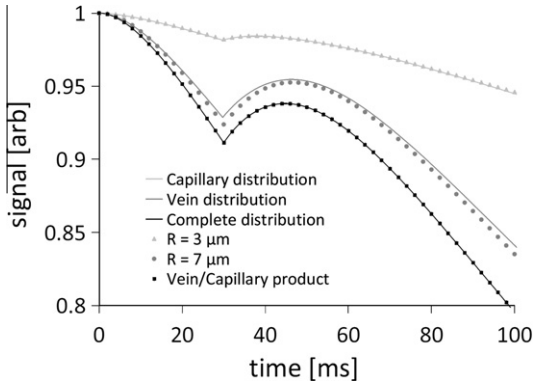

Fig. 10. The signal from the complete distribution of vessel radii is shown to exactly correspond to the product of signals from separate capillary and vein fractions. The agreement between signal from the capillary and vein fractions is also compared to their mean radius values $R = 3$ μm and $R = 7$ μm respectively. Capillaries behave more similar to a network with a single radius than veins due to their symmetrical R distribution.

From Fig. 7 one can see the range of vessel radii for which each of the models described are effective at estimating the various tissue parameters. For physiologically common values of vessel radii, the most accurate estimations of *OEF* and dCBV are made by the Yablonskiy and Haacke model for the FID sequence. This suggests that improvements to the qBOLD method may be possible be switching to the FID sequence, rather than the SE sequence which is currently favoured [4,25,32]. It is slightly surprising that the model of Kiselev and Posse can only estimate *OEF* accurately for vessels larger than 20 μm in radius for the SE sequence. The explanation lies in the fact that the approximation of the signal decay as G^2t^3 is only valid in an extremely narrow range of times [22]. It turned out that the restrictions of diffusion by the blood vessel surfaces modified the t^3 time dependence of MR signal by generating an additional negative term proportional to $t^{7/2}$, as appears in Eqs. (18) and (24) in [22]. Due to the presence of such a $t^{7/2}$ term, the time interval where the cubic term adequately describes the signal behaviour is very small.

As *OEF* and ζ appear only as a product in the Sukstanskii and Yablonskiy model, these parameters are indistinguishable and this model alone cannot be used to separate them. The fact that separate information on *OEF* and dCBV is not available when the phase distribution is close to Gaussian suggests that long echo times are more effective for quantitative BOLD.

Another application of diffusive BOLD models is vessel size imaging (VSI) [11] which exploits the different sensitivity of GE and SE sequences to vessel radii shown in Fig 6. Currently this is achieved by measuring the apparent diffusion coefficient (ADC) and the ratio of contrast-related relaxation rate changes for GE and SE sequences. These data are then typically analysed by applying the Kiselev and Posse model for SE and the Yablonskiy and Haacke model for FID. Recent research has shown that the resulting vessel radius estimates disagree with microscopy measures by a factor of 6–8 [33]. The results in Fig. 6 suggest that this could be due to the invalid assumption of slow diffusion for $R < 20$ μm.

In order to produce a model that is accurate for the physiological range of vessel radii we turned to a phenomenological approach. It is possible to fit Eq. (25) to our simulation results with an extremely high level of accuracy (see Fig. 8). In fact the typical fitting residual is $\sim 10^{-5}$, which is low enough to suggest that the form of the model has some significance.

The parameters that result from fitting the phenomenological model to the simulation results describe smooth curves that are exponential for low values of *OEF* or *TE* and linear for high values (see Fig. 9). Fitting the expression in Eq. (26) to these curves yielded the values in Tables 1 and 2 which can be used to generate a phenomenological BOLD model that could be used to fit data for quantitative BOLD or to assess the accuracy of future diffusive BOLD models.

Inspection of the variation of terms in Eq. (25) with *OEF* (which scales with $\delta\omega$) and *TE* shows that a parameter with units of time (presumably the diffusion time) is needed to make A_2 and A_3 dimensionless. Further exploration of this model over varied vessel radii and diffusion rates may allow this parameter to be elucidated.

In Fig. 10 we show that the signal from separate fractions of the radius distribution can be combined to reproduce the signal for the full distribution (in agreement with [19]). This suggests several further improvements to the quantitative BOLD method. By calculating the signal from the capillaries and veins separately, the vessel types could be given different values of *OEF*, ζ, T_2, permeability and blood hematocrit. In addition, the signal attenuation caused by veins and capillaries could be separately calculated by whichever model is the most accurate and then the results combined.

Several semi-phenomenological models have previously been proposed for description of the MR signal in the presence of magnetic field inhomogeneities [26,39]. The model by Stables et al. [40]

makes the same Gaussian approximation as that of Sukstanskii and Yablonskiy but also makes the additional assumption that the correlation function is a simple exponential, $G(t) = \exp(-t/t_c)$, where t_c is a correlation time. Under these assumptions the signal time-course around the spin-echo is:

$$s(t) = \exp\left[-\overline{\Delta\omega^2}t_c^2\left(2\exp\left[-\frac{TE}{2t_c}\right] + 2\exp\left[-\frac{2t-TE}{2t_c}\right] - \exp\left[-\frac{t}{t_c}\right] + \frac{t}{t_c} - 3\right)\right], \tag{31}$$

where $\overline{\Delta\omega^2} = 3/5\delta\omega^2\zeta$. While it provides a simple and attractive way to describe MR signal, it also introduces a phenomenological parameter t_c with undetermined relationship to system properties. Also, as it was demonstrated by Jensen and Chandra [41], the correlation function does not satisfy exponential behaviour. If the assumption of a simple exponential correlation function were valid, the parameter t_c could be found by fitting this equation to simulated time-courses (in the range of validity of the Gaussian approximation). Although this was not found to be the case, our phenomenological model in Eq. (25) has a similar "structure" as the model in Eq. (31).

Correctly accounting for diffusion in models of the BOLD mechanism represents a major step towards understanding the basis of the phenomenon. To further improve on the model there are a number of additional considerations, the most obvious being the validity of infinite cylinder approximation. Although it is difficult to see how the branching structure of a vessel network could be incorporated into a mathematical model, it would be relatively straight-forward to grow simulated networks using either the finite element [34] or finite perturber [35] method. The results could then be fitted with a phenomenological model as was performed in this study, or related back to one of the analytical models. A similar approach could be used to account for the compartmentalisation of deoxyhaemoglobin by red blood cells within the blood vessels. This study has focussed on the extravascular signal, where the assumption that cylinders have uniform susceptibility has been shown to be accurate [36]. The intravascular contribution may however be strongly dependent on intravascular compartmentalisation of deoxyhaemoglobin (and hence intravascular diffusion). Phenomenological equations for blood signal were proposed previously [37] based on experimental measurements.

The existence of cylinder orientation anisotropy could be easily accounted for in either analytical models or simulations. In the static dephasing regime, for example, vessel orientation anisotropy can be accounted for by inserting an orientation distribution function when orientation averaging is performed. In Ref. [27]) the standard deviation of vessel orientations is found to be ~0.87 rad across the healthy human brain. Assuming a normal distribution, the form of the resulting signal is similar to that under the random cylinder model, however the apparent *OEF* is shifted from its true value by up to 8% depending on mean vessel orientation.

Finally there is the assumption of isotropic diffusion. We know from diffusion MRI studies that there is significant diffusion anisotropy in white matter [38] (although rates are still well described by a Gaussian distribution). As expected, diffusion anisotropy in an isotropically oriented vessel network has very little effect on the signal (results not shown). However, there may well be a significant effect on the signal when diffusion anisotropy is combined with vessel orientation anisotropy.

5. Conclusion

Existing models of the BOLD contrast mechanism are able to accurately calculate signal only for networks of either capillaries or large veins. The diffusion approximations of the BOLD models were shown to have varying impacts on the ability to measure tissue parameters, depending on choice of model and sequence. In this paper we have introduced a new, phenomenological model that is extremely accurate for the case of blood vessels modelled as long uniform cylinders with the physiological distribution of radii. This model could be used in BOLD data analysis or to test the effectiveness of future analytical models.

Acknowledgments

Simulations were run on the Supercomputer of Washington University. We also thank the Engineering and Physical Sciences Research Council and the Medical Research Council (MRC G0600986 WBIC acute brain injury collaborative grant) and NIH Grant R01 NS 055963 (D.A.Y. and A.L.S.) for funding this research.

References

[1] S. Ogawa, T.M. Lee, A.R. Kay, D.W. Tank, Brain magnetic-resonance-imaging with contrast dependent on blood oxygenation, Proc. Natl Acad. Sci. U. S. A. 87 (24) (1990) 9868–9872.
[2] S. Ogawa, R.S. Menon, D.W. Tank, S.G. Kim, H. Merkle, J.M. Ellermann, K. Ugurbil, Functional brain mapping by blood oxygenation level-dependent contrast magnetic-resonance-imaging – a comparison of signal characteristics with a biophysical model, Biophys. J. 64 (3) (1993) 803–812.
[3] D.A. Yablonskiy, E.M. Haacke, Theory of NMR signal behavior in magnetically inhomogeneous tissues – the static dephasing regime, Magn. Reson. Med. 32 (6) (1994) 749–763.
[4] X. He, D.A. Yablonskiy, Quantitative BOLD: mapping of human cerebral deoxygenated blood volume and oxygen extraction fraction: default state, Magn. Reson. Med. 57 (1) (2007) 115–126.
[5] X. He, M. Zhu, D.A. Yablonskiy, Validation of oxygen extraction fraction measurement by qBOLD technique, Magn. Reson. Med. 60 (4) (2008) 882–888.
[6] C.P. Derdeyn, T.O. Videen, K.D. Yundt, S.M. Fritsch, D.A. Carpenter, R.L. Grubb, W.J. Powers, Variability of cerebral blood volume and oxygen extraction: stages of cerebral haemodynamic impairment revisited, Brain 125 (2002) 595–607.
[7] W.D. Heiss, Best measure of ischemic penumbra: positron emission tomography, Stroke 34 (10) (2003) 2534–2535.
[8] S. Davda, T. Bezabeh, Advances in methods for assessing tumor hypoxia in vivo: implications for treatment planning, Cancer Metastasis. Rev. 25 (3) (2006) 469–480.
[9] J.L. Tatum, G.J. Kelloff, R.J. Gillies, J.M. Arbeit, J.M. Brown, K.S.C. Chao, J.D. Chapman, W.C. Eckelman, A.W. Fyles, A.J. Giaccia, R.P. Hill, C.J. Koch, M.C. Krishna, K.A. Krohn, J.S. Lewis, R.P. Mason, G. Melillo, A.R. Padhani, G. Powis, J.G. Rajendran, R. Reba, S.P. Robinson, G.L. Semenza, H.M. Swartz, P. Vaupel, D. Yang, B. Croft, J. Hoffman, G.Y. Liu, H. Stone, D. Sullivan, Hypoxia: importance in tumor biology, noninvasive measurement by imaging, and value of its measurement in the management of cancer therapy, Int. J. Radiat. Biol. 82 (10) (2006) 699–757.
[10] V.G. Kiselev, R. Strecker, S. Ziyeh, O. Speck, J. Hennig, Vessel size imaging in humans, Magn. Reson. Med. 53 (3) (2005) 553–563.
[11] I. Tropres, S. Grimault, A. Vaeth, E. Grillon, C. Julien, J.F. Payen, L. Lamalle, M. Decorps, Vessel size imaging, Magn. Reson. Med. 45 (3) (2001) 397–408.
[12] J. Dennie, J.B. Mandeville, J.L. Boxerman, S.D. Packard, B.R. Rosen, R.M. Weisskoff, NMR imaging of changes in vascular morphology due to tumor angiogenesis, Magn. Reson. Med. 40 (6) (1998) 793–799.
[13] K.M. Schmainda, S.D. Rand, A.M. Joseph, R. Lund, B.D. Ward, A.P. Pathak, J.L. Ulmer, M.A. Baddrudoja, H.G.J. Krouwer, Characterization of a first-pass gradient-echo spin-echo method to predict brain tumor grade and angiogenesis, Am. J. Neuroradiol. 25 (9) (2004) 1524–1532.
[14] J.L. Boxerman, P.A. Bandettini, K.K. Kwong, J.R. Baker, T.L. Davis, B.R. Rosen, R.M. Weisskoff, The intravascular contribution to FMRI signal change – Monte-Carlo modeling and diffusion-weighted studies in-vivo, Magn. Reson. Med. 34 (1) (1995) 4–10.
[15] J. Martindale, A.J. Kennerley, D. Johnston, Y. Zheng, J.E. Mayhew, Theory and generalization of Monte Carlo models of the BOLD signal source, Magn. Reson. Med. 59 (3) (2008) 607–618.
[16] K. Uludag, B. Muller-Bierl, K. Ugurbil, An integrative model for neuronal activity-induced signal changes for gradient and spin echo functional imaging, Neuroimage 48 (1) (2009) 150–165.
[17] B.F. Kjolby, L. Ostergaard, V.G. Kiselev, Theoretical model of intravascular paramagnetic tracers effect on tissue relaxation, Magn. Reson. Med. 56 (1) (2006) 187–197.
[18] J.O. Eichling, M.E. Raichle, R.L. Grubb, K.B. Larson, M.M. Terpogossian, In vivo determination of cerebral blood-volume with radioactive oxygen-15 in monkey, CircRes 37 (6) (1975) 707–714.
[19] V.G. Kiselev, S. Posse, Analytical model of susceptibility-induced MR signal dephasing: effect of diffusion in a microvascular network, Magn. Reson. Med. 41 (3) (1999) 499–509.

[20] V.G. Kiselev, S. Posse, Analytical theory of susceptibility induced NMR signal dephasing in a cerebrovascular network, Phys. Rev. Lett. 81 (25) (1998) 5696–5699.
[21] A.L. Sukstanskii, D.A. Yablonskiy, Gaussian approximation in the theory of MR signal formation in the presence of structure-specific magnetic field inhomogeneities, J. Magn. Reson. 163 (2) (2003) 236–247.
[22] A.L. Sukstanskii, D.A. Yablonskiy, Gaussian approximation in the theory of MR signal formation in the presence of structure-specific magnetic field inhomogeneities: effects of impermeable susceptibility inclusions, J. Magn. Reson. 167 (1) (2004) 56–67.
[23] M. Abramowitz, I.A. Stegum, Handbook of Mathematical Functions with Formulas, Graphs, and Mathematical Tables, fourth ed., National Bureau of Standards, Washington, DC, 1965.
[24] W.R. Bauer, W. Nadler, M. Bock, L.R. Schad, C. Wacker, A. Hartlep, G. Ertl, Theory of coherent and incoherent nuclear spin dephasing in the heart, Phys. Rev. Lett. 83 (20) (1999) 4215–4218.
[25] C.H. Ziener, T. Kampf, G. Melkus, V. Herold, T. Weber, G. Reents, P.M. Jakob, W.R. Bauer, Local frequency density of states around field inhomogeneities in magnetic resonance imaging: effects of diffusion, Phys. Rev. E 76 (2007) (3).
[26] J.D. Dickson, T.W.J. Ash, G.B. Williams, S.G. Harding, T.A. Carpenter, D.K. Menon, R.E. Ansorge, Quantitative BOLD: the effect of diffusion, J. Magn. Reson. Imaging 32 (4) (2010).
[27] F. Lauwers, F. Cassot, V. Lauviers-Cances, P. Puwanarajah, H. Duvernoy, Morphometry of the human cerebral cortex microcirculation: general characteristics and space-related profiles, Neuroimage 39 (3) (2008) 936–948.
[28] D.A. Yablonskiy, Quantitation of intrinsic magnetic susceptibility-related effects in a tissue matrix: phantom study, Magn. Reson. Med. 39 (1998) 417–428.
[29] T.L. Davis, K.K. Kwong, et al., Calibrated functional MRI: mapping the dynamics of oxidative metabolism, Proc. Natl. Acad. Sci. U. S. A. 95 (4) (1998) 1834–1839.
[30] S.G. Kim, E. Rostrup, et al., Determination of relative CMRO2 from CBF and BOLD changes: significant increase of oxygen consumption rate during visual stimulation, Magn. Reson. Med. 41 (6) (1999) 1152–1161.
[31] H.Z. Lu, C.G. Zhao, Y.L. Ge, K. Lewis-Amezcua, Baseline blood oxygenation modulates response amplitude: physiologic basis for intersubject variations in functional MRI signals, Magn. Reson. Med. 60 (2) (2008) 364–372.
[32] M.C. Sohlin, L.R. Schad, Susceptibility-related MR signal dephasing under nonstatic conditions: experimental verification and consequences for qBOLD measurements, J. Magn. Reson. Imaging 33 (2) (2011).
[33] C.T. Farrar, W.S. Kamoun, C.D. Ley, Y.R. Kim, S.J. Kwon, G.P. Dai, B.R. Rosen, E. di Tomaso, R.K. Jain, A.G. Sorensen, In vivo validation of MRI vessel caliber index measurement methods with intravital optical microscopy in a U87 mouse brain tumor model, Neuro-Oncol. 12 (4) (2010) 341–350.
[34] J.P. Marques, R.W. Bowtell, Using forward calculations of the magnetic field perturbation due to a realistic vascular model to explore the BOLD effect, NMR Biomed. 21 (6) (2008) 553–565.
[35] A.P. Pathak, B.D. Ward, K.M. Schmainda, A novel technique for modeling susceptibility-based contrast mechanisms for arbitrary microvascular geometries: the finite perturber method, Neuroimage 40 (3) (2008) 1130–1143.
[36] A.F. Frohlich, L. Ostergaard, V.G. Kiselev, Theory of susceptibility-induced transverse relaxation in the capillary network in the diffusion narrowing regime, Magn. Reson. Med. 53 (3) (2005) 564–573.
[37] W.M. Spees, D.A. Yablonskiy, M.C. Oswood, J.J.H. Ackerman, Water proton MR properties of human blood at 1.5 Tesla: Magnetic susceptibility, T-1, T-2, T-2$*$ and non-Lorentzian signal behavior, Magn. Reson. Med. 45 (4) (2001) 533–542.
[38] P.J. Basser, C. Pierpaoli, Microstructural and physiological features of tissues elucidated by quantitative-diffusion-tensor MRI, J. Magn. Reson. Ser. B 111 (3) (1996) 209–219.
[39] D.S. Novikov, V.G. Kiselev, Transverse NMR relaxation in magnetically heterogeneous media, J. Magn. Reson. 195 (1) (2008) 33–39.
[40] L.A. Stables, R.P. Kennan, J.C. Gore, Asymmetric spin-echo imaging of magnetically inhomogeneous systems: Theory, experiment, and numerical studies, Magn. Reson. Med. 40 (3) (1998) 432–442.
[41] J.H. Jensen, R. Chandra, NMR relaxation in tissues with weak magnetic inhomogeneities, Magn. Reson. Med. 44 (1) (2000) 144–156.